Influence of interfacial elasticity on liquid entrainment in thin foam films

Gigi Lin, John M. Frostad,[*,†] and Gerald G. Fuller[*]
Chemical Engineering, Stanford University, California, USA

(Received 30 September 2017; published 6 November 2018)

The influence of interfacial elasticity on the rate of liquid drainage from gas-liquid interfaces is a subject that has encouraged prolific scientific work on coalescence and film stability. Elucidating this relationship is important for the design of surfactant mixtures where the amount of liquid content of the foam is critical for the aesthetics and/or effectiveness of the product. However, contradictory theoretical predictions exist with regard to how surface elasticity may influence thin-film dynamics. In this work, interferometric studies are performed to measure the liquid film entrainment between a bubble and an air-liquid interface in response to systematic variations of the surface elasticity. The surface elasticity is varied by adjusting the age of the interface or by adjusting the bulk concentration of a surface-active molecule known to form highly elastic surface layers. Surprisingly, the results indicate the absence of a strong relationship between the surface shear elasticity and the entrainment of liquid in foam films. In addition, qualitative differences are observed between the shapes of foam films with differences in interfacial shear viscosity, with no net effect on liquid entrainment under the conditions studied.

DOI: 10.1103/PhysRevFluids.3.114001

I. INTRODUCTION

Foams are dispersions of gas in liquid and are well known to the public because of their ubiquity in food beverages [1–3] pharmaceuticals [4–7], and commercial cleaning products, as well as to industry for their utility in removing organic pollutants from industrial waste streams [8,9]. Each application requires different foam characteristics that often vary as a function of time [10,11].

Drainage of liquid from the interstitial spaces of a foam, that is, through thin films, Plateau borders, and nodes, results in the separation of the liquid from the gas phase [12,13]. Films can thin as the result of gravitationally and/or capillary-driven flows. The consequent volume and rate of liquid loss from the foam can impact a consumer's experience with food and beverages, such as the tactile sensation of froth in a freshly poured glass of beer. A foam can also experience a gradual growth of the average bubble size, known as coarsening, due to the coalescence of adjacent bubbles or from diffusive mass transfer of gas from small bubbles to large bubbles [14]. Because the present work aims to investigate the initial liquid fraction of a newly formed foam, the discussion here will exclude coarsening effects and will primarily focus on drainage processes.

When discussing the rate of drainage of liquid from a foam, one should note that this process is strongly influenced by the presence and composition of surface-active species (surfactants, proteins, polymers, etc.), which facilitate foam formation by lowering the energy required to create excess area. The process of selecting a surfactant for a particular foam should be accompanied by consideration of its physicochemical properties, including its bulk and interfacial diffusivities,

[*]Corresponding authors: john.frostad@ubc.ca; ggf@stanford.edu
[†]Current address: Chemical and Biological Engineering, University of British Columbia and Food Science, University of British Columbia, Vancouver, British Columbia, Canada.

adsorption-desorption kinetics at interfaces, pC_{20} value (measure of surfactant efficiency), and micellar structure, as well as its safety, chemical stability, and ecotoxicity profile [15–18]. The interfacial viscoelasticity conferred by surfactant-adsorbed layers may also affect the stress response to shearing and dilational deformation (expansion and compression) during drainage [19].

The desire to understand how surfactants influence drainage rates and liquid entrainment in foams and emulsions has inspired researchers over many decades. One simple approach used by many groups is to assume that the interface has a range of mobility that is restricted by Marangoni stresses that resist surface-tension gradients, with the limiting case of immobile corresponding to zero tangential velocity [20–24]. Under this assumption, the dynamics of foam interfaces should be agnostic of surfactant type, provided that enough surfactant is present to immobilize the interface. However, Frostad *et al.* found significant quantitative differences in both foam density and liquid entrainment in individual films for solutions of simple water-soluble surfactants at concentrations above the critical micelle concentration [18]. Furthermore, data from Bhamla *et al.* show that films bound by viscoelastic interfaces can drain more slowly than what is predicted by the immobile limit [25].

A more comprehensive approach would therefore include not only considerations of Marangoni stresses but also the effects of structure in the adsorbed layer. Measurement of the surface rheology is one attempt to account for these structural effects in terms of liquidlike (viscous) and solidlike (elastic) properties that are believed to arise from intermolecular forces at the interface. The material properties that describe the viscous and elastic properties of the surface are defined relative to the deformation applied to the surface (e.g., dilational and shear) and change dramatically with surfactant type. For example, under shear deformation, the commonly studied small-molecule surfactants such as sodium dodecyl sulfate (SDS) exhibit immeasurably small surface shear viscosities (smaller than 0.01 μN (s/m) [10^{-8} N (s/m)] for SDS) [26], while proteins, which are much larger and conformationally complex, can exhibit significant surface shear viscosities ranging from 10^{-5} to 1 N (s/m) [27–29], with the values depending on the unfolding characteristics of the protein and other testing parameters [19].

Under dilational deformation, on the other hand, small-molecule surfactants like SDS display a measurable elasticity, though this is merely due to the surface-tension gradient effects (also known as the Gibbs-Marangoni effect) and normally referred to as the Gibbs elasticity. Alternatively, proteins such as those studied in this paper may have strong intermolecular interactions and exhibit dilational viscosity and elasticity that greatly exceed the resistance to deformation associated with the Gibbs-Marangoni effect [30,31]. In particular, we aim to study interfaces that are predominantly elastic as opposed to viscoelastic or purely viscous.

Using variations of these two frameworks for modeling interfaces, previous researchers have attempted to determine the impact that interfacial elasticity will have on the dynamics in foams and other multiphase systems, sometimes with contradictory results. Within the construct of the mobility framework, Zapryanov *et al.* developed a hydrodynamic model for predicting the time for the thin film between coalescing liquid droplets to drain to a final thickness. Their model predicts an increase in the drainage time with a decrease in mobility caused by an increase in the Gibbs elasticity and with an increase in the sum of dilatational and shear viscosity within a range of 10^{-6}–10^{-3} Pa m s [32]. In agreement with this prediction, Tambe and Sharma numerically calculated the rate of drainage of an axisymmetric, plain-parallel, horizontal film between two droplets that shows decreased drainage rates with increasing Gibbs elasticity. They also considered the effect of increasing the dilatational surface elasticity and total surface viscosity using a generalized Maxwell model with a continuous distribution of relaxation times and predicted that an increase in either the elasticity or viscosity of the surface will increase the thickness of the entrained film at a given reference time [33].

In contrast, a recent hydrodynamic model presented by Ramachandran and Leal predicts a decrease in the drainage time of a thin film between two vesicles or capsules with an increase in the area expansion modulus of the vesicle membrane [34]. Because the vesicle membrane is modeled as a thin shell, its area expansion modulus can be thought of as analogous to the interfacial elasticity of a two-dimensional fluid interface. This is in contrast again to a previous theoretical study from

Biswas and Haydon, which predicts that interfacial elasticity would not have a significant impact on the drainage rate of thin films bounded by viscoelastic interfaces [35].

Many experimental studies have also been conducted on viscoelastic interfaces by examining film stability against coalescence and, to a lesser extent, film drainage and liquid entrainment [36–39]. Unfortunately, experimental work has not yet resolved the contradictory theoretical predictions outlined above. Part of the reason for this is that developing methods to characterize the viscoelasticity of interfaces is still an active area of research [31,40–42]. Another reason is that it is difficult to produce interfaces with well-controlled properties.

Protein-laden interfaces are often studied because they have been found to produce a wide range of viscoelastic behavior, though it is often time dependent (usually increasing with time) [19,43,44], and may be disrupted by the addition of small-molecule and polymeric surfactants to reduce the viscoelasticity [45,46]. For example, Van Aken found that increasing the ratio of low-molecular-weight surfactants to protein β-lactoglobulin increased the rate of emulsion film rupture [37]. Similarly, Blomqvist *et al.* discovered that adding nonionic polymeric surfactant F127 significantly reduced the dilatational and shear elasticity of lactoglobulin solutions and decreased the time for the film to drain to an equilibrium thickness, but did not affect the long-term stability of the residual film due to long-range steric interactions provided by F127 layers [47]. Both studies suggest that increasing viscoelasticity ought to slow film drainage but were not sufficient to systematically validate prior theoretical predictions.

These lingering contradictions in the theoretical models compel our study, which aims to systematically vary the surface elasticity in thin-film drainage experiments. In the present work, the central hypothesis is that the surface elasticity influences the volume of liquid entrained in a thin film and its subsequent drainage. It is important to emphasize that in this study the elasticity arises from intermolecular interactions among surface-active species that either irreversibly adsorb to the interface and impart gel-like characteristics or engage in other strong intermolecular bonding at the surface. Thus, the interfaces will not be directly comparable to small-molecule surfactant solutions where the Gibbs elasticity is the primary source of dilational elasticity. To quantify the entrained volume we utilize an interferometry-based technique that we refer to as a dynamic fluid-film interferometer (DFI). Similar to other instruments of this type, it uses reflectance interferometry to generate three-dimensional (3D) representations of foam film profiles [18,48].

Instruments that use reflectance interferometry to measure the thicknesses of microscopic films are well documented in literature, such as the well-known Scheludko cell (and modernized versions thereof) [49–53]. The DFI used in this study is an extension of the i-DDrOP apparatus developed previously in our laboratory [25] and is somewhat similar to the apparatuses used by Sett *et al.* [54] and Berg *et al.* [55]. However, it is important to note that the bubble radius in the present work is at least an order of magnitude smaller in size (bubble or solid surface) than in these studies. This point is critical to our analysis since the smaller bubble size favors capillary-pressure-driven drainage over the gravitationally-driven drainage studied previously. Additionally, the DFI used for the present study has the advantage of providing independent control over bubble size, approach velocity, and film size [18].

In this study, we restrict our attention to the drainage of a thin film formed between a bubble and a bulk air-solution interface. Our work follows recently published work using the same experimental technique, which demonstrated correlations between the volume of liquid entrained in the thin film and the film thinning rates to the densities of freshly formed foams of the same surfactant solutions [18]. This underscores the utility of simple thin-film measurements for studying foam behavior. In this study the elasticity of the interfaces is systematically varied while attempting to hold all other variables constant. We primarily studied bovine serum albumin (BSA) because it is a commonly studied globular protein known to unfold and form interfacial networks with significant elasticity at air-liquid interfaces [44,56]. To supplement the studies with BSA, we used escin, a monodesmosidic triterpenoid saponin molecule (one sugar chain with three hydrophobic residues) known to form surface layers with significant surface elasticity arising from extensive hydrogen bonding [57,58].

II. METHODS

A. Experimental overview

To modulate the interfacial rheology of the air-liquid interface, we vary the bulk surface-active species concentration or the surface age in separate sets of experiments. The general process is outlined as follows. First, the bulk air-water and bubble interfaces are aged simultaneously under quiescent conditions with the bubble far away from the bulk interface. Then the distance between the bubble and the bulk interface is decreased until the two surfaces deform and entrain a thin film of liquid. The difference between the aging studies and concentration studies is that the former varies the aging time at constant bulk concentration of the surface-active species, whereas the latter varies the bulk concentration of surface-active species while maintaining a constant aging time.

For this study, the BSA concentration studies were conducted for surfaces aged 40 min and the surface aging studies were conducted at a constant BSA concentration of 0.96 mM. Complementary to the set of BSA experiments, the escin studies utilized only surface aging studies and were completed at a constant escin concentration of 4.4 mM. These concentration and surface aging times were chosen to yield a range of surface elasticity values for comparison in investigating the effect on thin-film properties for the molecules studied.

B. Materials

Several batches of lyophilized BSA (molecular weight equal to 66 kDa) were purchased from Sigma Aldrich (catalog No. A7906, CAS: 9048-46-8, $\geqslant$98% purity). Solutions of 1.5×10^{-3} mM (0.1 mg/mL) to 0.96 mM (64 mg/mL) were made by dissolving measured masses of the lyophilized powder with phosphate-buffered solution (1$\times$ from Corning Cellgro: catalog No. 21-040-CV) within glass vials before gently stirring the contents with a stir bar for at least an hour. When not in use, the solutions were kept refrigerated at 4 °C. All solutions were made with an ionic strength of 0.16M. The concentration of the solutions was verified using UV-vis absorption at 280 nm on a NanoDrop instrument and the built-in permittivity constant for BSA.

The escin saponin was purchased as a powder from Alfa Aesar (catalog No. J66968, CAS: 6805-41-0, 98% purity, formula weight 1131.26). The structure of a saponin is inverted from common surfactants since a saponin molecule possesses a hydrophobic head called an aglycone linked to one or several sugar chains by glycoside bonds, which contrasts with the hydrophilic head and hydrophobic tail found in a common surfactant. Solutions of escin were made from powdered escin added to phosphate-buffered solution (1$\times$ from Corning Cellgro: catalog No. 21-040-CV) in glass vials. The solutions were sonicated in a liquid bath for at least half an hour to dissolve the escin. Afterward, the solution was filtered through a 0.22-μm and 13-mm-diam Millipore Durapore PVDF membrane filter (catalog No. SLGV013SL) to remove heterogeneous materials, including observed colored insoluble impurities present in the solution and thus minimize variation in the turbidity of the solutions. When not in use, the solutions were kept refrigerated at 4 °C. All solutions were made with an ionic strength of 0.16M.

C. Surface tension measurements

A standard, pendant drop tensiometer method was utilized to measure the surface tension of the air-liquid interfaces. It is important to note that while this method is valid for pure liquid-liquid interfaces, previous studies have found increasing error of the fitted Laplace shape to pendant drops with increasing surface pressure that is associated with the liquid-solid transition of the interface [59,60]. Usually, the solidification is observed by the interfacial compression and expansion of the drop. The present measurements monitor only the apparent surface tension changes at a constant volume that are due to adsorption and conformational changes of surface-active species at the stationary air-liquid interface. Considering this, we collected the data with a focus on identifying the relative magnitudes of the apparent surface tension and trends in the time evolution at different bulk concentrations.

For surface-tension measurements, a droplet on the order of 100 μL is dispensed through a syringe needle of outer diameter 2.413 mm connected to a 1-mL syringe. In each case, the first two droplets are discarded to purge the system. A disposable plastic cuvette filled with 1 mL of distilled water is placed around the pendant drop to maintain a more controlled and humidified environment to mitigate evaporation effects. Back illumination of the droplet with a source of uniform diffuse lighting produces sharp contrast at the droplet edges. An Edmund Optics camera with a Nikon F-Bayonet lens is used to capture images of the droplet, which are then analyzed with an iterative shape-fitting algorithm. For convenience, we report the measurements here as the surface pressure, defined as $\pi = \gamma_0 - \gamma(t)$, in which γ_0 is the surface tension of the pure liquid and $\gamma(t)$ is the dynamic surface tension. In these experiments, the droplet formed from solution already has surface-active species adsorbed at the interface at early times and for this reason the plotted surface pressure appears as finite near $t = 0$. These early-time data are not needed for the present experiments in which aging times are on the order of tens of minutes.

D. Bulk viscosity measurements

A standard Cannon-Fenske glass viscometer of size 50 was utilized to measure the kinematic viscosities of the solutions. The viscometer constant for the specific viscometer was verified with the measured efflux time of water and its known viscosity at a specified temperature. Before use, the viscometer is rinsed several times with distilled water and ethanol before it is dried by flowing air through the glassware. Then, prior to filling, the viscometer walls are primed with several milliliters of the sample. A consistent volume of 5 mL of solution was used for each measurement and the fluid was assumed to be Newtonian.

E. Interfacial rheology measurements

We characterized the interfacial shear rheology of the interfacial protein layers with an AR-G2 rheometer (TA Instruments, New Castle, DE) and a Du Noüy ring attachment made of platinum-iridium wire (CSC Scientific, Fairfax, VA, catalog No. 70542000) of an inner diameter of 0.46 in. and an outer diameter of 0.5 in. [61]. Before each experiment, the Du Noüy ring is flame cleaned to remove any organic residues.

A Teflon trough was constructed to hold the solution, with a 0.5-mm step size at the outer Teflon wall such that the radius of the outer wall with the step is 1.04 in. The trough is filled with about 4.5 mL of solution such that the liquid level reaches the step and the air-liquid interface is pinned. After each experiment, the Teflon trough is cleaned by rinsing with both water and ethanol, scrubbed with Q-tips, and allowed to air dry before the next use.

For all aging and bulk concentration experiments, the Peltier plate is kept at 25 °C. The rheological characterization experiments performed in this study monitored the interfacial rheology over time with oscillatory shear measurements. After an initial equilibration time of 1 min, the interface was periodically sheared at an angular frequency of 0.5 rad/s and 1% strain. We found that rheological experiments at other frequencies exhibit similar qualitative trends. Additionally, strain sweeps performed on BSA-adsorbed interfaces indicated that the utilized 1% strain was within the linear viscoelastic regime. In comparison, the interfacial shear rheology of escin was conducted at a lower strain of 0.1% for the deformation response to remain within the linear viscoelastic regime.

Interfacial dilational rheology measurements were not performed in this study due to the inherent difficulty in obtaining systematic measurements for this system. Nevertheless, we make the assumption that the intermolecular interactions that result in high shear elasticity will also result in a high dilational elasticity as well. This assumption is based on the theoretical prediction that, for predominantly elastic interfaces, the dilational modulus will be proportional to the shear modulus, which has in fact been observed in experiments for other globular protein solutions [19,27,29,35,44,62]. Note that this is only expected to be the case for our BSA solutions and will not necessarily hold for the escin solutions or other viscoelastic interfaces in general (such

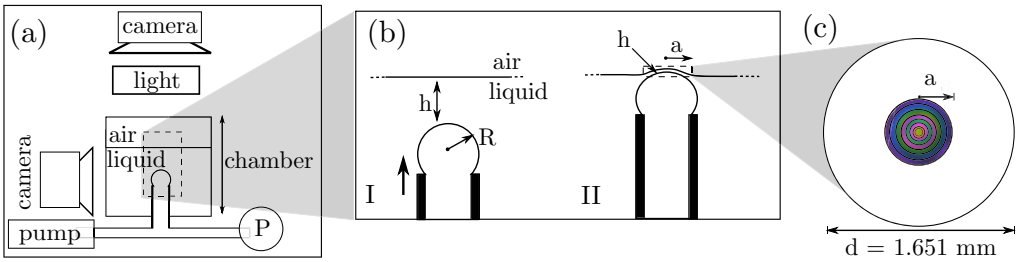

FIG. 1. (a) Overview of the DFI used for thin-film measurements: two cameras, a light source, a syringe pump, a pressure transducer (labeled as P), and a chamber capable of vertical translational motion. (b) Diagram of the process for a typical thin-film experiment. (I) Initially, the bubble and bulk air-solution interface are stationary and separated. (II) The interfaces are brought into contact, resulting in deformation of the two interfaces that traps a thin film of liquid. The term a denotes the film radius, R the bubble radius, and h the film thickness (on the order of 0.1–1 μm). (c) Top view of the interferometry patterns that arise from liquid entrainment in the thin film. The term d denotes the capillary outer diameter.

as phospholipid bilayers). Finally, because we are varying the interfacial rheology without changing the molecular composition, we expect other factors that may influence interfacial rheology to be constant.

F. Dynamic thin-film measurements

The DFI is an apparatus that can be used to characterize thin-film properties premised upon the interference of light reflected from boundaries of a thin liquid film. As shown in Fig. 1(a), the DFI consists of a syringe pump (Harvard Apparatus Pump 11 Elite catalog No. HA1100W) fitted with a gas-tight 100-μL syringe (Hamilton catalog No. 1710CX) that forms the bubble in a custom-machined Delrin chamber with a 6-mL capacity that is open to the atmosphere. Narrow gas-tight plumbing (tubing: IDEX PEEK 1/16-in. o.d. $\times$ 0.030-in. i.d. catalog No. 1533L) conveys air from the syringe to the 16G blunt-tipped capillary needle (1.194-mm i.d., 1.651-mm o.d.) that forms the bubble in the chamber. A motor (Newport catalog No. TRA12PPD, catalog No. SMC100PP) attached to the solution chamber moves up or down to change the relative distance between the bubble and interface, and a pressure transducer (Omegadyne catalog No. PX409-10WGUSBH) provides the option of measuring the pressure within the bubble. Two orthogonally positioned cameras provide imaging of the top view (Imaging Development Systems catalog No. UI-3060CPC) and side view (ThorLabs catalog No. DCU223) of the chamber. Illumination from a light source (CCS Inc. catalog No. LAV-80SW2) that induces reflection interference is conditioned with a dichroic filter (Edmund Optics catalog No. 87245) with passbands at 457, 530, and 628 nm. The equipment is operated via a custom-written MATLAB script.

1. Protocol for a typical DFI experiment

The general operation of the DFI is shown in Fig. 1(b). The experiments are performed by adding approximately 5 mL of solution to the Delrin chamber. A bubble of approximately 1.10 μL is formed at the tip of the capillary, which is submerged in the solution. At this point the bubble is positioned a distance of one bubble radius below the upper air-liquid surface via translation of the chamber and then aged as needed for the particular experiment. After aging is complete, the pressure inside the bubble is monitored for 10 s to ensure that the bubble volume is stable against environmental disturbances. The chamber is then moved down at a speed of 150 $\mu\mathrm{m\,s^{-1}}$ for all experiments, causing the bubble and bulk surface to interact. The chamber is moved instead of the capillary to ensure that the bubble is a fixed distance away from the camera lens and remains in focus. During the approach of the bubble and top surface, hydrodynamic and capillary forces cause the deflection of the upper surface and compression of the bubble that results in the entrainment of a

liquid film between the surfaces. The formation of the thin liquid film gives rise to the interferometry patterns shown in Fig. 1(c).

2. Drainage of thin films

After the initial formation of a liquid film between the surfaces, the radius of the film continues to expand as the bubble compresses into the interface, continuing until the motion of the chamber is stopped. In contrast, the mean and maximum thicknesses of the film are observed to decrease monotonically with time. As a consequence of the simultaneous increase in film radius and decrease in film thickness, the volume of the liquid film increases with time to reach a maximum value after the formation of the initial film. If we assume that the liquid film is cylindrical in shape, the volume can be simply written as $V = \pi a^2 h_m$, where V is the film volume, a is the radial extent of the film, and h_m is the mean film thickness. The rate of change in volume, or the film thinning rate dV/dt, can then be written as

$$\frac{dV}{dt} = \pi a^2 \frac{dh_m}{dt} + 2\pi a h_m \frac{da}{dt}.$$

The time at which the maximum volume occurs depends on the balance of the two terms on the right-hand side of the equation. The first term describes the drainage of the film, which in these experiments is always negative. In comparison, the second term, which describes fluid capture due to the expansion of the film, is initially positive at early experiment times and then zero after the chamber stops moving. For relatively small elevation velocities, the expansion of the film is small and the volume maximum occurs while the film is still expanding [18]. In these experiments, the elevation velocity of the chamber is sufficiently high that the maximum in the volume always occurs exactly when the film stops expanding, which is convenient for analysis. Because changes in normal-stress and tangential-stress boundary conditions impact the drainage dynamics, this technique affords a convenient way to quantify the effect of changing the interfacial elasticity on the drainage process.

3. Analysis of reflectance interferometry data

The interference data recorded as videos during thin-film experiments are converted to film thicknesses with the Color Analyzer software (version 2.3.1.1) written with PYTHON and QT [18]. The software first generates a colormap unique to the system's hardware configuration and film material. Then a graphical user interface is used to process individual video frames. To analyze an individual video frame, the user manually selects a color on the colormap and matches it to pixels along each distinct region of color in the interference pattern. Linear interpolation of user-selected points is used to create a 3D projection of the film onto a planar surface. On average, the manual matching process results in an estimated error of about ± 15 nm, though it can be slightly lower or higher depending on the user's ability to discriminate colors [18].

To quantify liquid entrainment, a single video frame from each experiment is analyzed for the period while the thin film is still expanding when it reaches a radius of $112 \pm 1\mu$m. Trends in mean film thickness are used for comparing the effects of the different experimental conditions because they change in a manner similar to trends in the film volume, yet are less sensitive to small variations in film radius. Measurements of mean film thickness are calculated as the spatial average of the film thickness over the film region, and the reported error bars represent a standard deviation based on at least two replicates at each condition.

III. RESULTS OF BSA STUDIES

A. Interfacial properties of BSA

Figure 2 shows a time-sweep plot of the surface pressure for several BSA concentrations. It is accompanied by Fig. 3, which shows time-sweep plots of the surface shear elastic and viscous

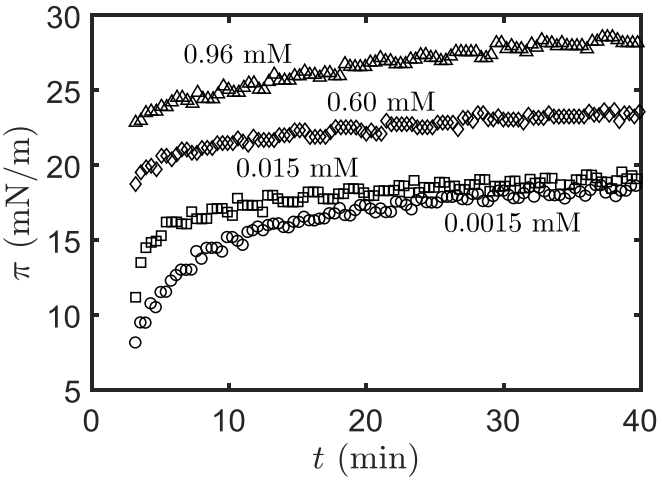

FIG. 2. Representative dynamic air-solution surface pressure behavior as a function of time for a range of bulk BSA concentrations (1.5×10^{-3} mM [0.1 mg/mL], 1.5×10^{-2} mM [1 mg/mL], 0.60 mM [40 mg/mL], and 0.96 mM [64 mg/mL]).

moduli for several BSA concentrations. Both figures indicate that the surface properties evolve more rapidly at initial times before approaching approximately constant values at longer times. Both figures also show that increasing concentration results in systematic increases in surface pressure, elastic modulus, and viscous modulus. We assume that the transition from a rapid change in surface pressure to a slower increase over long periods of time indicates that adsorption of BSA is completed and further changes are due to structural changes in the protein and/or protein network. Therefore, we assume that effects due to adsorption kinetics can be avoided by aging the interface for at least 5 min.

Examination of Fig. 3 reveals a wide spread in the value of the surface shear moduli across concentrations and aging time, with values on the order of 10 mM/m for G_s' and 1 mM/m for G_s''. For the first 50 min, the elastic modulus and viscous modulus of interfaces at higher bulk BSA concentrations exhibit the greatest increase among the investigated concentrations. At longer times, the elastic modulus shows more modest growth and the viscous modulus approaches a constant

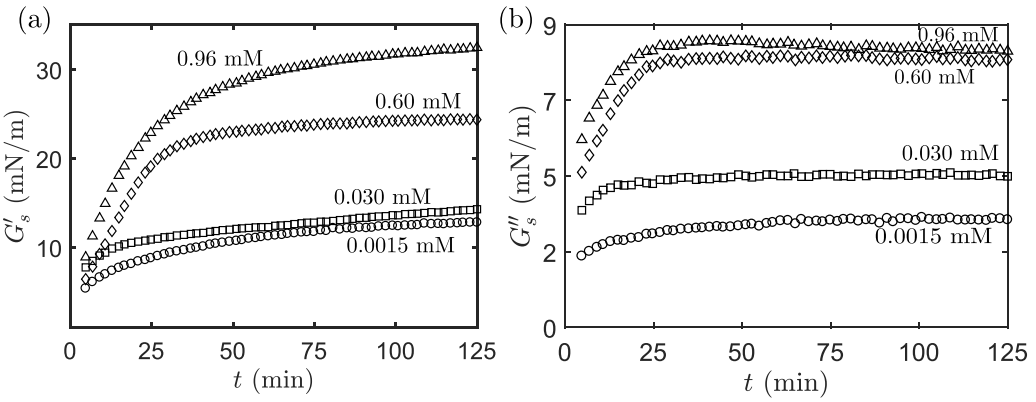

FIG. 3. Time t sweep of the interfacial shear elastic modulus [(a) elastic modulus G_s' and (b) viscous modulus G_s''] for several bulk concentrations of BSA. Subsequent figures will compare the trends in interfacial shear rheology at either a surface aging time of 40 min for concentration-dependent studies or at a bulk BSA concentration of 0.96 mM for surface aging-dependent studies.

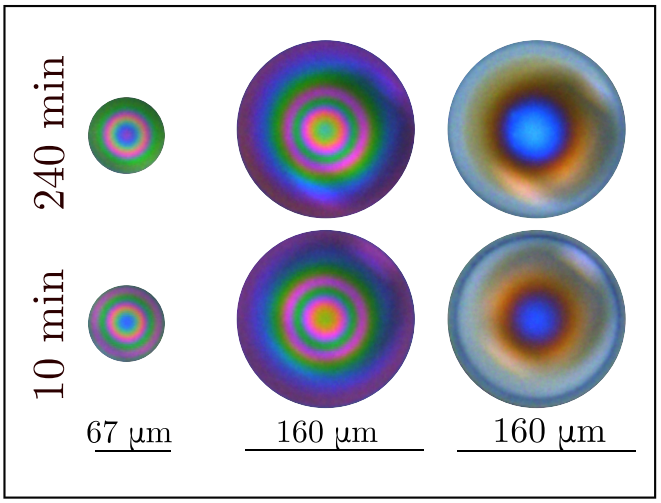

FIG. 4. Effect of aging on the film drainage for 0.96 mM BSA films. From left to right, the interferometry patterns are shown at three representative drainage time points: 1.46 s before the chamber stops moving, the time at which the chamber stops moving (corresponding to maximum film volume), and 59.9 s after the chamber stops. The bottom row corresponds to air-solution surfaces aged for 10 min, whereas the top row corresponds to surfaces aged for 240 min. Note the axisymmetry in film shape.

value. In general, the BSA-adsorbed interfaces are predominantly elastic and the elastic modulus is 3–4 times larger than the viscous modulus in most cases. Because the rheology of the interfaces is sensitive to changes in both bulk concentration and surface aging time, either parameter can be used to tune the elasticity of the interface.

B. BSA film properties

Next we examine results from the thin-film experiments. Qualitatively, Fig. 4 shows that BSA films exhibit axisymmetric shapes starting from initial film formation and throughout film drainage for all studied surface aging times. Notably, there is an absence of asymmetric surface flows driven by Marangoni stresses across all investigated concentrations, which is consistent with the relatively high elasticity measured for these BSA-adsorbed surfaces. The absence of surface mobility is also consistent with the Koehler *et al.* observations of approximately zero surface velocities for protein surfactants at aqueous foam surfaces [63].

Figure 5(a) shows that the mean film thickness (taken at the same point in time during the drainage process) exhibits a modest increase with increasing bulk BSA concentration for a fixed surface aging time of 40 min. The lowest concentration in the plot is 1.5×10^{-3} mM (rather than zero) and the mean film thickness increases by about 150 nm as the bulk concentration is increased from the lowest concentration to 0.96 mM. Compared to the effect of increasing bulk concentration, the effect of increasing surface aging time results in a smaller increase in mean film thickness, about 20 nm, over the range of investigated aging times at 0.96 mM BSA, shown in Fig. 5(b).

The changes in film thickness can now be compared to the interfacial elasticity. To accomplish this, both sets of data are normalized by their respective "initial" values at the lowest bulk concentration (Fig. 6) and at the shortest aging time (Fig. 7). In Fig. 6 we observe that the surface shear elastic and viscous moduli increase strongly as a function of concentration and each increases to about 3 times the initial values over the concentration range. The trends in the surface pressure, bulk viscosity, and mean film thickness reveal that each of the three quantities increase to approximately 1.5 times their initial values over the same concentration range. Overall these results show a positive correlation between the bulk concentration and the surface characteristics. However,

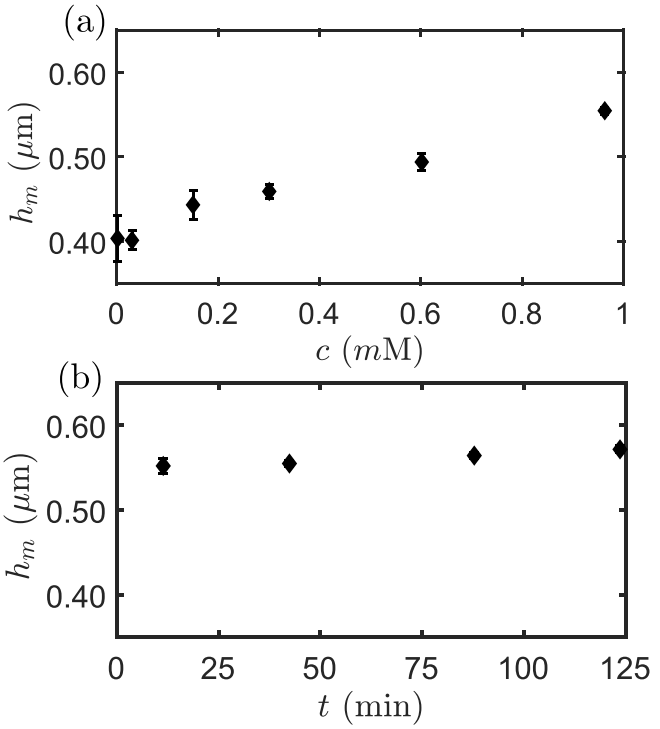

FIG. 5. (a) Mean film thickness h_m as a function of bulk BSA concentration c at a surface aging time of $t = 40$ min, with a lower concentration limit of 1.5×10^{-3} mM, scientific notation. (b) Mean film thickness h_m as a function of surface aging time t at a bulk BSA concentration c of 0.96 mM.

since the film thickness is expected to be influenced by bulk viscosity and surface pressure as well as the interfacial rheology, these results alone are insufficient to determine the relationship between film thickness and interfacial elasticity. In contrast, the data from the experiments with surface aging at a fixed concentration have the same bulk viscosity and can be used to help clarify the dependence.

Figure 7 shows the normalized surface elastic and viscous moduli along with the mean film thickness and surface pressure. The bulk viscosity is not shown because its value is independent of time. By comparing these data to Fig. 6, we see that the bulk viscosity appears to be primarily responsible for the observed increase in film thickness with increasing concentration. This is not unexpected since we know from lubrication theory that the thinning rate of a film (for rigid surfaces) is inversely proportional to bulk viscosity [64].

We also see that a large increase in surface elasticity with aging time and with a relatively constant surface viscous modulus and surface pressure is accompanied by only a tiny increase in mean film thickness. This suggests that the liquid entrained in foam films is in fact only very weakly correlated to surface elasticity. This result is not very intuitive for three reasons. First, according to the prevailing thinking in terms of interfacial mobility, most theoretical studies cited in the Introduction anticipated the increased elasticity to be accompanied by a decreased mobility and hence slower drainage and a thicker film. Second, one would expect instead that a higher interfacial shear elasticity for a predominantly elastic interface would result in a higher dilational elasticity (though there may be exceptions to this), which would effectively increase the capillary pressure in the film due to the increased resistance to dilational deformation and speed up the rate of drainage [34]. Third, experimental results have suggested that increasing the value of the Gibbs elasticity results in significant increases in entrained liquid in foam films under gravitational drainage [54].

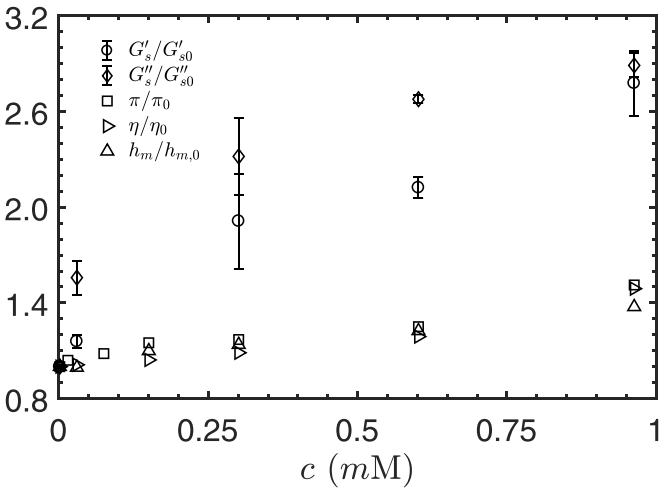

FIG. 6. Concentration dependence of interfacial and bulk properties in BSA solutions normalized by initial values at 1.5×10^{-3} mM. The circles and diamonds correspond to the normalized surface shear elastic G_s' and shear viscous modulus G_s'', respectively. Squares, right-facing triangles, and upward-facing triangles correspond to normalized surface pressure π, normalized bulk viscosity η, and normalized mean thickness h_m, respectively.

Although our findings appear to refute the majority of theoretical predictions, one theoretical prediction by Biswas and Haydon [35] does predict a negligible dependence on elasticity in film drainage, with a stronger dependence on surface viscosity. However, their model is based on thin shell theory for a viscoelastic sheet as a model for the interface (the interface is referred to as the film in that paper) and does not include the hydrodynamics of drainage within the thin film. Because

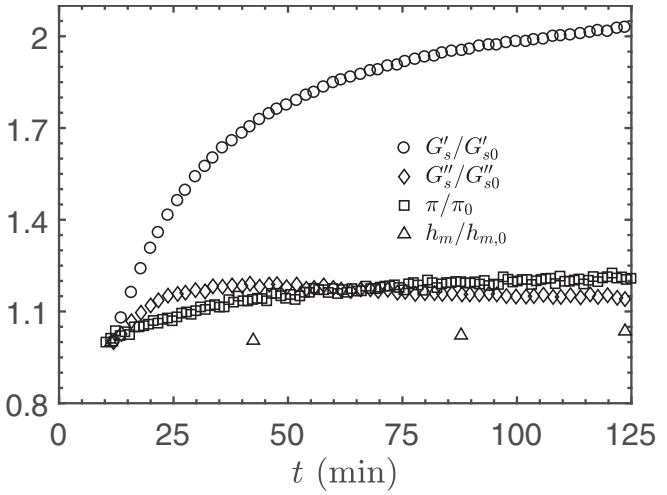

FIG. 7. Temporal behavior for several interfacial parameters and the mean film thickness in a solution of 0.96 mM [64 mg/mL] BSA, with the data normalized by initial values at a 10-min aging time. The circles and diamonds denote the normalized surface shear elastic G_s' and shear viscous modulus G_s'', respectively. Squares correspond to the normalized surface pressure π and the upward-facing triangles correspond to the normalized mean thickness h_m.

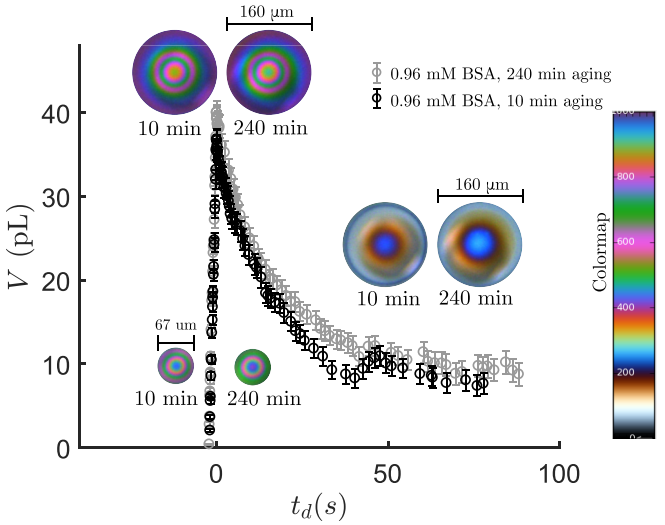

FIG. 8. Film volume V as a function of thin-film drainage time t_d for 0.96 mM BSA surfaces aged for 10 min ($G_s' = 14$ mN/m, black circles) and for 240 min ($G_s' = 33$ mN/m, gray circles) prior to film formation. Note that the time axis is shifted such that $t_d = 0$ corresponds to the occurrence of the maximum film volume, which in this case also corresponds to the time at which the chamber stops moving. Accompanying the volume curves are three pairs of interferometry patterns corresponding to approximately $t_d = -1.46$, 0, and 59.9 s. Each pair compares the interferometry patterns for a film aged briefly, 10 min, (left of the pair) and for a prolonged period, 240 min (right of the pair).

of this, it is difficult to use their analysis to point to a qualitative mechanism that might explain the present findings, but their analysis may inspire future theoretical developments.

C. Drainage behavior of aged BSA surfaces

While the mean film thickness at the maximum film volume captures the aggregate influence of the hydrodynamic boundary conditions into a single measurement and is therefore useful for comparison, it does not tell the whole story. Another important metric is how the film thins as a function of time. Figure 8 compares the film volume over time for BSA surfaces with low (at 10-min aging) and high (at 240-min aging) surface shear elasticities. The time $t_d = 0$ corresponds to when the film reaches its maximum volume, which in this case corresponds to when the chamber stops moving. Each pair of the interferometric patterns (inset in the figure) corresponds to a different time point in the film drainage process. Comparison of the volume curves and the interference patterns at initial, intermediate, and long drainage times shows only modest differences in the maximum amount of entrained liquid and in the rate of film drainage. The one notable difference observed is a dip in volume at around 40 s for the 10-min aged surfaces; however, this was found to be the result of a fluctuation in the bubble size due to a pressure fluctuation in the laboratory air-handling system.

Another way of understanding the drainage of the film is to examine the film thickness as a function of drainage time. Many researchers have investigated this relationship, resulting in a variety of differing predictions for the minimum film thickness as a function of time [54,55,65,66]. Figure 9 shows the maximum, mean, and minimum film thickness for the same data as in Fig. 8 along with a few examples of the predicted scaling relations from the literature (for the assumption of immobile interfaces) [67,68]. Unfortunately, the uncertainty in the data for the minimum film thickness is too large to make a confident statement about the experimental drainage rate, but two sample power-law predictions ($h_{\min} \sim t^{-1/2}$ and $h_{\min} \sim t^{-2/3}$ [67]) are shown for comparison anyway. On the other hand, the maximum and mean film thicknesses appear to approach power-law behavior at long times

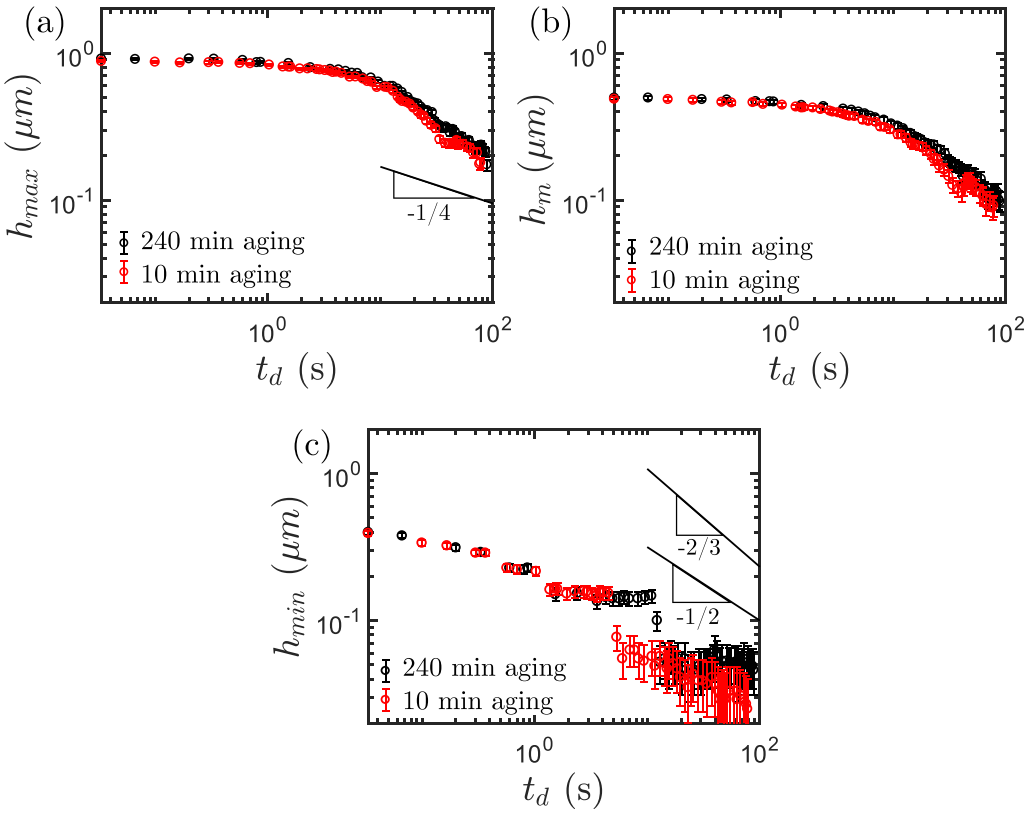

FIG. 9. (a) Maximum film thickness $h_{\max}$, (b) mean film thickness h_m, and (c) minimum film thickness $h_{\min}$ as a function of thin-film drainage time t_d for BSA surfaces aged for short (10 min, red circles) and long (240 min, black circles) times before film formation. Note that the time axis is shifted such that $t_d = 0$ corresponds to the occurrence of the maximum film volume.

(with slopes of approximately -0.55 and -0.62, respectively), but when compared to a prediction for maximum thickness ($h_{\max} \sim t^{-1/4}$ [68]) the data clearly do not match well. As with the volume entrained, there is very little difference in the maximum, mean, and minimum film thickness for the two different aging times. This further supports the observation that changes in surface elasticity have little impact on the film drainage process under these conditions.

Other researchers have made similar experimental measurements of film thickness versus time [23,53,54,69,70]. However, the present results are not expected to be directly comparable because of significant differences in the interfacial rheology of the systems studied and/or significant differences in the length scale and driving force for drainage (e.g., gravity vs capillarity) of the film. Indeed, even if one compares the results of two studies such as those of Bhamla *et al.* (drainage from a film on a solid sphere) and of Sett *et al.* (drainage from a bubble), in which the length scales of the film curvature are the same, one sees different drainage behavior ($t^{-1/2}$ vs t^{-1}). These differences underscore the need for additional research in this area.

IV. RESULTS OF ESCIN STUDIES

The preceding section examined the use of BSA to modulate and measure the impact of interfacial elasticity on film drainage. In this section, another surface-active species, escin, will be used to help determine if the findings are unique to BSA. To avoid changing the bulk viscosity, only

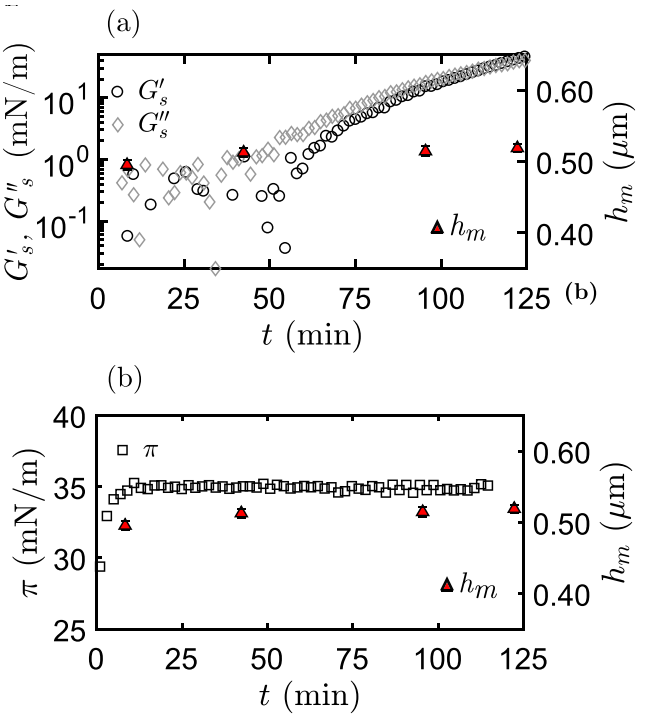

FIG. 10. (a) Comparison of the surface shear elastic modulus G'_s and the surface shear viscous modulus G''_s (left y axis) with the mean film thickness h_m (right y axis) for 4.4 mM escin. (b) Comparison of dynamic surface pressure π (left y axis) with mean film thickness h_m (right y axis) for 4.4 mM escin.

surface aging will be used to vary the interfacial elasticity of an escin solution with a concentration of 4.4 mM. We selected escin to study alongside BSA because other researchers reported that it can form predominantly elastic layers at air-water interfaces [58]. Unfortunately, our measurements show that the escin used in this study does not form predominantly elastic interfaces (see the next section), presumably due to the natural variability of escin and purity differences between suppliers. Nevertheless, the results show interesting trends.

A. Escin film properties

Figure 10 shows that, as with BSA, both the interfacial shear rheology and surface pressure increase with time. The surface pressure, shown in Fig. 10(b), exhibits an initial increase with time before saturating at a constant value within about 10 min. In contrast to BSA, the escin surface layers exhibit interfacial shear viscous moduli that are on the same order as the interfacial shear elastic moduli over the examined aging times, indicating a viscoelastic rather than a predominantly elastic film. Nevertheless, the shear elasticity values for escin range from near zero (below the resolution of the instrument) to 50 mN/m, which one might expect to span the range from low tangential mobility to high tangential mobility.

Interestingly, even over this very large range of interfacial shear moduli, the mean film thickness as shown in Figs. 10(a) and 10(b) changes negligibly. This trend is consistent with the changes in mean film thickness observed with BSA films, but in this case is even more significant because at the shortest aging time the magnitudes of the elastic and viscous moduli are below the resolution of the rheometer. At present, we prefer not to attempt to provide a rationalization for this observation as this would be a worthy topic for future research; however, we may at least conclude that these

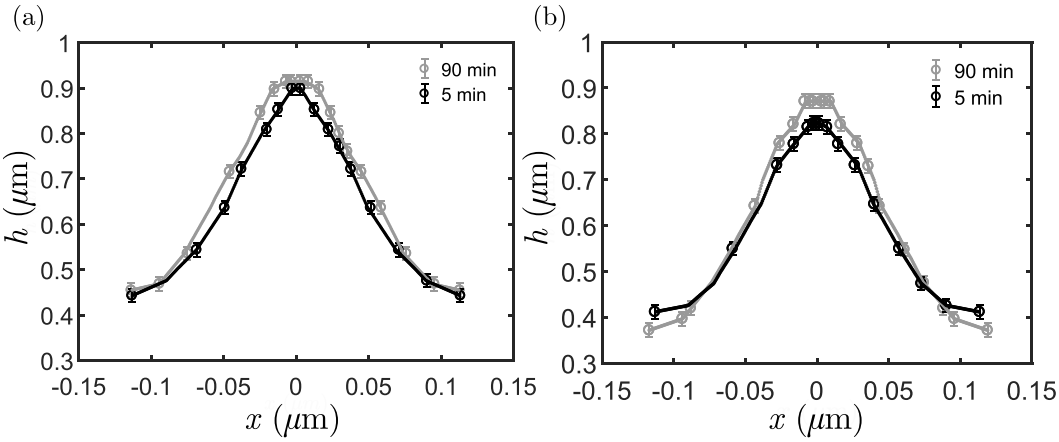

FIG. 11. Comparison of film contours arising from 5-min (black) and 90-min (gray) aged surfaces for (a) 0.96 mM BSA and (b) 4.4 mM escin. The outermost points in the figures demarcate the edge of the film as observed in the interference patterns. The circles represent user-selected points, connected by lines of interpolated points.

data do not contradict the findings for BSA in which interfacial elasticity shows an extremely weak influence on entrainment of liquid in foam films of this type.

B. BSA and escin film shape

Apart from the mean film thickness and film volume, our experimental apparatus also enables us to examine the film shape. Because of the axisymmetric character of these films we can look at the cross-sectional profile as shown in Fig. 11. Note that for these plots, the outermost points shown in each contour demarcate the boundary of the film beyond which the film thickens too rapidly with increasing radial position to be resolved by the camera.

For films of 0.96 mM BSA, we see a marginal thickening throughout the film that is more pronounced within the central region of the film (the dimple) as surface aging is increased. On the other hand, films of 4.4 mM escin show a more noticeable change in shape with increasing surface age, consisting of an increase in thickness in the center along with a thinning at the outer edge of the film. This suggests that even though the films show very little change in mean film thickness, the viscoelastic nature of the escin films produces qualitatively different drainage dynamics than the predominantly elastic BSA films. This observation underscores the importance of accounting separately for viscous and elastic contributions to the mechanical behavior of the interface. This also strengthens the finding that surface elasticity has a negligible impact on thin-film drainage dynamics relative to other properties.

V. CONCLUSION

The goal of this work is to experimentally quantify how interfacial elasticity influences the rate of liquid drainage from films between gas-liquid interfaces and consequently affects the density of freshly formed foams. Elucidating this relationship is important for the rational design of surfactant mixtures that achieve specific foam properties, especially in applications such as beer foam, medicated foams, and cosmetic foams, where the initial liquid density of the foam is critical for the aesthetics and/or effectiveness of the product.

The thin-film and surface characterization experiments performed in this study show only a very small correlation between surface shear elasticity and liquid entrainment in a freshly formed thin film of BSA and escin solutions. Not only did we observe minimal change in the mean film thickness

with large increases in the interfacial shear elasticity, but also we found minimal differences in time-dependent drainage behavior between fresh BSA surfaces (less elastic) and aged (more elastic) surfaces.

It was not possible to isolate the effect of surface elasticity for both BSA and escin because escin exhibited significant viscoelasticity in contrast to the predominantly elastic BSA surfaces. However, comparing the two systems led us to observe qualitative differences in the shape of the film between BSA and escin at comparable levels of surface elasticity that are masked in integrated metrics such as mean film thickness or film volume.

In conclusion, we find that use of surface-active species which form highly elastic surface layers will not necessarily result in films with greater initial liquid entrainment or slower film drainage as predicted by prior theoretical studies. Questions persist, and these findings motivate the need for further research, both experimentally and theoretically, to parse out the specific role of surface elasticity in dictating interfacial dynamics. It also highlights the usefulness of interferometry in probing thin-film dynamics.

ACKNOWLEDGMENTS

This work was partially funded by the National Science Foundation (USA) under Grant Number CBET-1435683. In addition, G. Lin acknowledges support from the Stanford Graduate Fellowship and J. M. Frostad acknowledges support from the Natural Sciences and Engineering Research Council Discovery Grant Program (Canada).

[1] A. D. Rudin, Measurement of the foam stability of beers, J. Inst. Brew. **63**, 506 (1957).
[2] J. M. Rodríguez Patino, C. Carrera Sánchez, and M. R. Rodríguez Niño, Implications of interfacial characteristics of food foaming agents in foam formulations, Adv. Colloid Interface Sci. **140**, 95 (2008).
[3] G. M. Campbell, *Aerated Foods*, 1st ed. (Elsevier, Amsterdam, 2016).
[4] D. Tamarkin, D. Friedman, and A. Shemer, Emollient foam in topical drug delivery, Expert Opin. Drug Del. **3**, 799 (2006).
[5] T. Kealy, A. Abram, B. Hunt, and R. Buchta, The rheological properties of pharmaceutical foam: Implications for use, Int. J. Pharm. **355**, 67 (2008).
[6] A. Arzhavitina and H. Steckel, Foams for pharmaceutical and cosmetic application, Int. J. Pharm. **394**, 1 (2010).
[7] Y. Zhao, S. A. Jones, and M. B. Brown, Dynamic foams in topical drug delivery What are topical foams? J. Pharm. Pharmacol. **62**, 678 (2010).
[8] R. Lemlich, Adsorptive bubble separation methods; foam fractionation and allied techniques, Ind. Eng. Chem. Res **60**, 16 (1968).
[9] J. Rubio, M. L. Souza, and R. W. Smith, Overview of flotation as a wastewater treatment technique, Miner. Eng. **15**, 139 (2002).
[10] A. Saint-Jalmes and D. Langevin, Time evolution of aqueous foams: Drainage and coarsening, J. Phys.: Condens. Matter **14**, 9397 (2002).
[11] A. Saint-Jalmes, Physical chemistry in foam drainage and coarsening, Soft Matter **2**, 836 (2006).
[12] S. A. Koehler, S. Hilgenfeldt, and H. A. Stone, A generalized view of foam drainage: Experiment and theory, Langmuir **16**, 6327 (2000).
[13] S. A. Koehler, S. Hilgenfeldt, and H. A. Stone, Foam drainage on the microscale: I. Modeling flow through single Plateau borders, J. Colloid Interface Sci. **276**, 420 (2004).
[14] S. Hilgenfeldt, S. A. Koehler, and H. A. Stone, Dynamics of Coarsening Foams: Accelerated and Self-Limiting Drainage, Phys. Rev. Lett. **86**, 4704 (2001).
[15] R. Zana, *Dynamics of Surfactant Self-Assemblies Micelles, Microemulsions, Vesicles and Lyotropic Phases* (CRC Press, Boca Raton, 2005).

[16] J. C. Berg, in *An Introduction to Interfaces and Colloids: The Bridge to Nanoscience* (World Scientific, Singapore, 2010), p. 107.
[17] M. J. Rosen and J. T. Kunjappu, *Surfactants and Interfacial Phenomena*, 4th ed. (Wiley, Hoboken, 2012).
[18] J. M. Frostad, D. Tammaro, L. Santollani, S. Bochner de Araujo, and G. G. Fuller, Dynamic fluid-film interferometry as a predictor of bulk foam properties, Soft Matter **12**, 9266 (2016).
[19] E. M. Freer, K. S. Yim, G. G. Fuller, and C. J. Radke, Shear and dilatational relaxation mechanisms of globular and flexible proteins at the hexadecane/water interface, Langmuir **20**, 10159 (2004).
[20] S. A. K. Jeelani and S. Hartland, Effect of interfacial mobility on thin-film drainage, J. Colloid Interface Sci. **164**, 296 (1994).
[21] S. L. Carnie, D. Y. C. Chan, C. Lewis, R. Manica, and R. R. Dagastine, Measurement of dynamical forces between deformable drops using the atomic force microscope. I. Theory, Langmuir **21**, 2912 (2005).
[22] J. M. Frostad, Fundamental investigations of phase separation in multiphase fluids, Ph.D. thesis, University of California, Santa Barbara, 2013.
[23] M. S. Bhamla, C. E. Giacomin, C. Balemans, and G. G. Fuller, Influence of interfacial rheology on drainage from curved surfaces, Soft Matter **10**, 6917 (2014).
[24] P. Yazhgur, E. Rio, F. Rouyer, F. Pigeonneau, and A. Salonen, Drainage in a rising foam, Soft Matter **12**, 905 (2016).
[25] M. S. Bhamla, C. Chai, M. A. Alvarez-Valenzuela, J. Tajuelo, and G. G. Fuller, Interfacial mechanisms for stability of surfactant-laden films, PLOS ONE **12**, e0175753 (2017).
[26] Z. A. Zell, A. Nowbahar, V. Mansard, L. G. Leal, S. S. Deshmukh, J. M. Mecca, C. J. Tucker, and T. M. Squires, Surface shear inviscidity of soluble surfactants, Proc. Natl. Acad. Sci. USA **111**, 3677 (2014).
[27] B. S. Murray and E. Dickinson, Interfacial rheology and the dynamic properties of adsorbed films of food proteins and surfactants, Food Sci. Technol. Int. **2**, 131 (1996).
[28] P. Dhar, Y. Cao, T. M. Fischer, and J. A. Zasadzinski, Active Interfacial Shear Microrheology of Aging Protein Films, Phys. Rev. Lett. **104**, 016001 (2010).
[29] V. Sharma, A. Jaishankar, Y.-C. Wang, and G. H. McKinley, Rheology of globular proteins: Apparent yield stress, high shear rate viscosity and interfacial viscoelasticity of bovine serum albumin solutions, Soft Matter **7**, 5150 (2011).
[30] L. E. Scriven, Dynamics of a fluid interface Equation of motion for Newtonian surface fluids, Chem. Eng. Sci. **12**, 98 (1960).
[31] A. P. Kotula and S. L. Anna, Regular perturbation analysis of small amplitude oscillatory dilatation of an interface in a capillary pressure tensiometer, J. Rheol. **59**, 85 (2015).
[32] Z. Zapryanov, A. K. Malhotra, N. Aderangi, and D. T. Wasan, Emulsion stability: An analysis of the effects of bulk and interfacial properties on film mobility and drainage rate, Int. J. Multiphase Flow **9**, 105 (1983).
[33] D. E. Tambe and M. M. Sharma, Hydrodynamics of thin liquid-films bounded by viscoelastic interfaces, J. Colloid Interface Sci. **147**, 137 (1991).
[34] A. Ramachandran and G. Leal, A scaling theory for the hydrodynamic interaction between a pair of vesicles or capsules, Phys. Fluids **22**, 091702 (2010).
[35] B. Biswas and D. A. Haydon, The coalescence of droplets stabilised by viscoelastic adsorbed films, Kolloid Z. Z. Polym. **185**, 31 (1962).
[36] D. E. Tambe and M. M. Shaftma, The effect of colloidal particles on fluid-fluid interfacial properties and emulsion stability, Adv. Colloid Interface Sci. **52**, 1 (1994).
[37] G. A. Van Aken, Competitive adsorption of protein and surfactants in highly concentrated emulsions: Effect on coalescence mechanisms, Colloid. Surf. A **213**, 209 (2003).
[38] D. Varade, D. Carriere, L. R. Arriaga, A. L. Fameau, E. Rio, D. Langevin, and W. Drenckhan, On the origin of the stability of foams made from catanionic surfactant, Soft Matter **7**, 6557 (2011).
[39] D. Harbottle, Q. Chen, K. Moorthy, L. Wang, S. Xu, Q. Liu, J. Sjoblom, and Z. Xu, Problematic stabilizing films in petroleum emulsions: Shear rheological response of viscoelastic asphaltene films and the effect on drop coalescence, Langmuir **30**, 6730 (2014).

[40] G. G. Fuller and J. Vermant, Complex fluid-fluid interfaces: Rheology and structure, Annu. Rev. Chem. Biomol. Eng. **3**, 519 (2012).
[41] T. Verwijlen, P. Moldenaers, and J. Vermant, A fixture for interfacial dilatational rheometry using a rotational rheometer, Eur. Phys. J. Spec. Top. **222**, 83 (2013).
[42] J. Tajuelo, J. M. Pastor, and M. A. Rubio, A magnetic rod interfacial shear rheometer driven by a mobile magnetic trap, J. Rheol. **60**, 1095 (2016).
[43] E. Dickinson, Adsorbed protein layers at fluid interfaces: Interactions, structure and surface rheology, Colloid. Surf. B **15**, 161 (1999).
[44] L. G. P. Pereira, H. W. Blanch, and C. J. Radke, Dilatational rheology of BSA conformers at the air/water interface, Langmuir **19**, 2349 (2003).
[45] M. Coke, P. J. Wilde, E. J. Russell, and D. C. Clark, The influence of surface-composition and molecular-diffusion on the stability of foams formed from protein surfactant mixtures, J. Colloid Interface Sci. **138**, 489 (1990).
[46] P. J. Wilde and D. C. Clark, The competitive displacement of β-lactoglobulin by Tween 20 from oil-water and air-water interfaces, J. Colloid Interface Sci. **155**, 48 (1993).
[47] B. R. Blomqvist, M. J. Ridout, A. R. Mackie, T. Wärnheim, P. M. Claesson, and P. Wilde, Disruption of viscoelastic beta-lactoglobulin surface layers at the air-water interface by nonionic polymeric surfactants, Langmuir **20**, 10150 (2004).
[48] M. S. Bhamla, C. Chai, N. I. Rabiah, J. M. Frostad, and G. G. Fuller, Instability and breakup of model tear films, Invest. Ophthalmol. Visual Sci. **57**, 949 (2016).
[49] A. Scheludko and D. Exerowa, Über den elektrostatischen druck in schaumfilmen aus wässerigen elektrolytlösungen, D. Kolloid Z. **165**, 148 (1959).
[50] L. G. Pereira, C. Johansson, H. W. Blanch, and C. J. Radke, A bike-wheel microcell for measurement of thin-film forces, Colloid. Surf. A **186**, 103 (2001).
[51] P. A. Wierenga, E. S. Basheva, and N. D. Denkov, Modified capillary cell for foam film studies allowing exchange of the film-forming liquid, Langmuir **25**, 6035 (2009).
[52] P. J. Beltramo, R. V. Van Hooghten, and J. Vermant, Millimeter-area, free standing, phospholipid bilayers, Soft Matter **12**, 4324 (2016).
[53] Y. Zhang, S. Yilixiati, C. Pearsall, and V. Sharma, Nanoscopic terraces, mesas, and ridges in freely standing thin films sculpted by supramolecular oscillatory surface forces, ACS Nano **10**, 4678 (2016).
[54] S. Sett, S. Sinha-Ray, and A. L. Yarin, Gravitational drainage of foam films, Langmuir **29**, 4934 (2013).
[55] S. Berg, E. A. Adelizzi, and S. M. Troian, Experimental study of entrainment and drainage flows in microscale soap films, Langmuir **21**, 3867 (2005).
[56] L. G. P. Pereira, C. Johansson, C. J. Radke, and H. W. Blanch, Surface forces and drainage kinetics of protein-stabilized aqueous films, Langmuir **19**, 7503 (2003).
[57] P. M. Dewick, *Medicinal Natural Produces: A Biosynthetic Approach*, 2nd ed. (Wiley, Chichester, 2002).
[58] K. Golemanov, S. Tcholakova, N. Denkov, E. Pelan, and S. D. Stoyanov, Remarkably high surface viscoelasticity of adsorption layers of triterpenoid saponins, Soft Matter **9**, 5738 (2013).
[59] S. M. I. Saad, Z. Policova, E. J. Acosta, and A. W. Neumann, Range of validity of drop shape techniques for surface tension measurement, Langmuir **26**, 14004 (2010).
[60] S. Knoche, D. Vella, E. Aumaitre, P. Degen, H. Rehage, P. Cicuta, and J. Kierfeld, Elastometry of deflated capsules: Elastic moduli from shape and wrinkle analysis, Langmuir **29**, 12463 (2013).
[61] S. Vandebril, A. Franck, G. G. Fuller, P. Moldenaers, and J. Vermant, A double wall-ring geometry for interfacial shear rheometry, Rheol. Acta **49**, 131 (2010).
[62] Z. Zhang, S. Barman, and G. F. Christopher, The role of protein content on the steady and oscillatory shear rheology of model synovial fluids, Soft Matter **10**, 5965 (2014).
[63] S. A. Koehler, S. Hilgenfeldt, E. R. Weeks, and H. A. Stone, Drainage of single Plateau borders: Direct observation of rigid and mobile interfaces, Phys. Rev. E **66**, 040601(R) (2002).
[64] L. G. Leal, *Advanced Transport Phenomena* (Cambridge University Press, Cambridge, 2007).
[65] J. M. Frostad, A. Paul, and L. G. Leal, Coalescence of droplets due to a constant force interaction in a quiescent viscous fluid, Phys. Rev. Fluids **1**, 033904 (2016).

[66] J. D. Berry and R. R. Dagastine, Mapping coalescence of micron-sized drops and bubbles, J. Colloid Interface Sci. **487**, 513 (2017).

[67] J. M. Frostad, J. Walter, and L. G. Leal, A scaling relation for the capillary-pressure driven drainage of thin films, Phys. Fluids **25**, 1 (2013).

[68] L. Bluteau, M. Bourrel, N. Passade-Boupat, L. Talini, E. Verneuil, and F. Lequeux, Water film squeezed between oil and solid: Drainage towards stabilization by disjoining pressure, Soft Matter **13**, 1384 (2017).

[69] T. T. Traykov, E. D. Manev, and I. B. Ivanov, Hydrodynamics of thin liquid films. Experimental investigation of the effect of surfactants on the drainage of emulsion films, Int. J. Multiphase Flow **3**, 485 (1977).

[70] A. A. Sonin, A. Bonfillon, and D. Langevin, Role of Surface Elasticity in the Drainage of Soap Films, Phys. Rev. Lett. **71**, 2342 (1993).